Proceedings of IMECE2008
2008 ASME International Mechanical Engineering Congress and Exposition
October 31-November 6, 2008, Boston, Massachusetts, USA

IMECE2008-68149

NUMERICAL STUDY IN WING TIP VORTEX FOR A MODIFIED COMMERCIAL BOEING AIRCRAFT

Ricardo Hernandez-Rivera
Department of Mechanical Engineering

Abel Hernandez-Guerrero
Department of Mechanical Engineering

Cuauhtemoc Rubio-Arana
Department of Mechanical Engineering

Raul Lesso Arroyo*
Department of Mechanical Engineering

Department of Mechanical Engineering, Universidad de Guanajuato.
C.P. 36730, Salamanca, Guanajuato, México, abelh@salamanca.ugto.mx.
*Department of Mechanical Engineering, Tecnológico de Celaya.

ABSTRACT

Recent studies have shown that the use of winglets in aircrafts wing tips have been able to reduce fuel consumption by reducing the lift-induced drag caused by wing tip vortex. This paper presents a 3-D numerical study to analyze the drag and lift forces, and the behavior of the vortexes generated in the wing tips from a modified commercial Boeing aircraft 767-300/ER. This type of aircraft does not contain winglets to control the wing tip vortex, therefore, the aerodynamic effects were analyzed adding two models of winglets to the wing tip. The first one is the vortex diffuser winglet and the second one is the tip fence winglet. The analyses were made for steady state and compressible flow, for a constant Mach number. The results show that the vortex diffuser winglet gives the best results, reducing the core velocity of the wing tip vortex up to 19%, the total drag force of the aircraft up to 3.6% and it leads to a lift increase of up to 2.4% with respect to the original aircraft without winglets.

1. INTRODUCTION

The vortex wake was first studied in detail in the early 60s after the appearance of the large transport aircraft (Boeing 747) which produces strong wing tip vortices [1]. The main reason was to estimate a safe separation distance required between two aircrafts following each other. A sufficient distance is necessary to minimize the risk of an aircraft of encountering a hazardous wake from a preceding aircraft and hence it is vital for flight safety. Nowadays, the main issue is aircraft traffic limitation: the objective is to optimize the air traffic which is expected to increase at a rate of 5% per year. Part of the solution is to increase the capacity of the existing airports by decreasing the vortex wake downstream of the aircraft.

The physics of the vortex formation in aircrafts is directly related to the wing, which is designed to create lift. In the case of a finite wing, the differences of pressures distribution on the top and bottom surfaces tends to curl the flow around the wing tips. The disturbances come from a spanwise component that bends the streamlines towards the wing root on the top surface and towards the tip of the wing on the bottom surface, as it is shown in Figure 1.

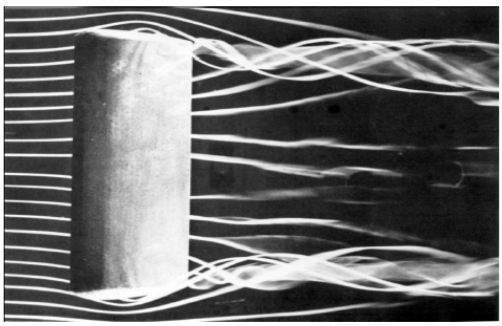

Figure 1. Formation of two tip vortices behind the wing [2].

Figure 2 shows the three different regions of the vortex wake of a real aircraft [1].

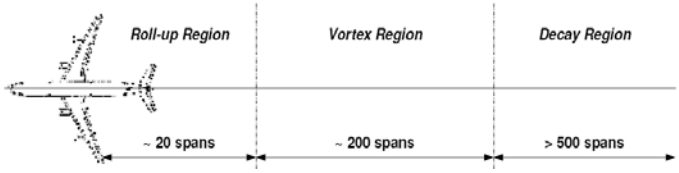

Figure 2. Vortex wake development and decay [3].

- Roll-up region (~20 spans, 5 sec flying time, 1 km). The vortex cores are formed and the thin shear layer defined as the vortex sheet accumulates most of the vorticity into the vortex cores.
- Vortex region (~200 spans, 1 min flying time, 10 km). The vortex system gradually drifts downwards and starts to decay. Atmospheric conditions have strong influence on the lifetime of the vortices, which can end in a vortex breakdown.
- Decay region (>500 spans, 1.5 min flying time, 20 km). In this region the remaining vortices disperse through viscous dissipation.

The strength of the trailing vortex can be expressed in terms of total wing circulation and the lift generated by the wing [1].

$$\Gamma = L/\rho V_o b \quad (1)$$

This equation shows that the vortex strength or circulation is proportional to the aircraft lift and inversely proportional to its speed. This leads to the conclusion that the wake is strongest for the take-off and landing configurations (the lift is maximum and the speed is minimum).

The streamwise vortices generate an induced velocity creating a downwash in the wing trailing edge, generating a resultant velocity for the airfoil section with an angle ϵ respect to the undisturbed free-stream [4]. Having the component of the induced velocity in the aerodynamic center, the velocity components are shown in Figure 3.

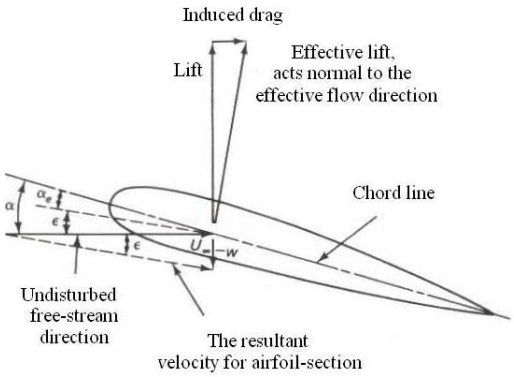

Figure 3. Induced flow in a subsonic airfoil [4].

The effective lift always acts normal to the resultant velocity. Due to the inclination of the resultant velocity with an angle ϵ, there will be a parallel force component with the free-stream direction called lift-induced drag.

The most direct way to reduce the lift-induced drag of a wing was suggested by Prandtl's elliptical wing result [5].

$$D_i = L^2/q\pi b^2 \quad (2)$$

The induced drag of a wing can be reduced by 10% simply by increasing the span by about 5%. However, increasing the wingspan, with a fixed wing area, increases the weight of the wing due to higher bending moments and a thinner, less efficient structure. Whereas the induced drag varies with $1/b^2$, the wing bending weight varies as b^3. Studies from NASA Langley concluded that winglets were preferred over span extensions [6].

One of the most often-cited approaches to induced drag reduction is the application of nonplanar lifting surfaces [5]. Figure 4 shows how the shape of the wake affects the minimum drag by illustrating the maximum span efficiencies for a range of concepts with fixed height and span. Note that the vertical extent of the system near the tips is the critical parameter and that, although the box plane represents the absolute minimum solution, many other concepts provide very similar drag reductions and show that spanwise camber is most effective near the tip [7].

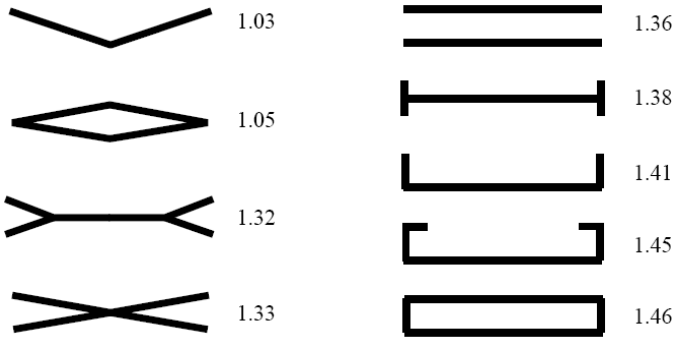

Figure 4. Span efficiencies for various optimally loaded nonplanar systems (h/b=0.2) [5].

Figure 5 shows some examples of different nonplanar systems as a function of height-to-span ratio in the relative vortex drag [5]. For fixed height and span, the minimum vortex drag is achieved with a box plane arrangement [8].

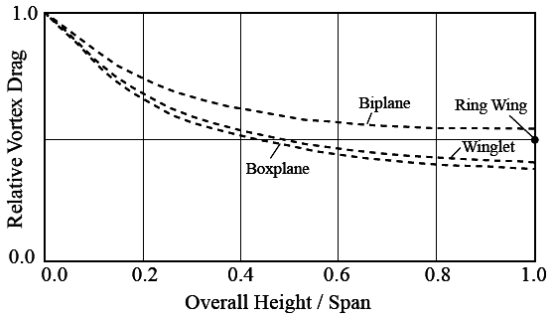

Figure 5. Induced drag variation with allowable height for nonplanar systems [5].

2. AIRCRAFT GEOMETRY

The geometry of the modified aircraft Boeing 767-300/ER under analysis is shown in Figure 6. The general dimensions are: fuselage length 56.1 m, maximum diameter of the fuselage 5.1 m, minimum diameter of the fuselage 4.7 m, wingspan 47.4 m, and an overall height of 13.6 m.

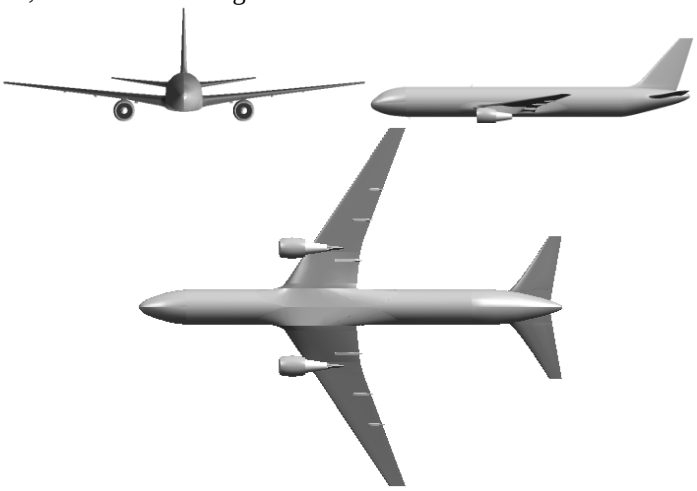

Figure 6. Aircraft under analysis.

The main wing has the supercritical airfoils shown in Figure 7 for the root chord and the tip chord respectively.

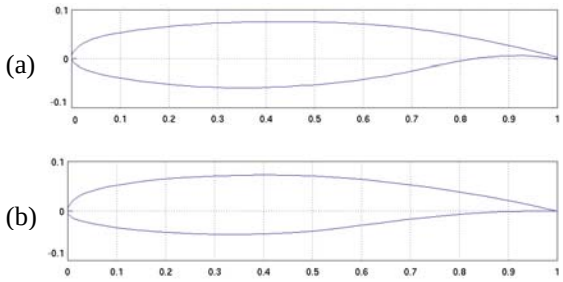

Figure 7. Supercritical airfoils for the main wing: (a) DFVLR R-4 for the root chord; (b) RAE (NPL) 5212 for the tip chord.

The geometric features for the main wing are shown in Table 1. The incidence angle was reduced linearly from the wing root to the wing tip.

Table 1. Geometric features for the main wing.

C_r	10.9 m	α_r	4º 15´	S	283.3 m^2
C_t	2.16 m	α_t	0 º	AR	8
Λ	31º 30´	ϕ	6 º	λ	0.19

The horizontal stabilizer has the supercritical airfoils shown in Figure 8 for the root chord and the tip chord respectively.

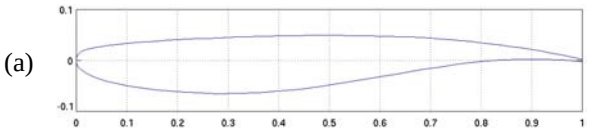

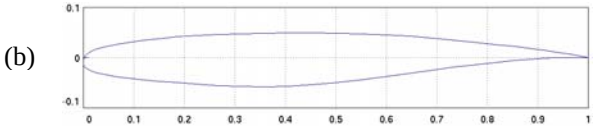

Figure 8. Supercritical airfoils for the horizontal stabilizer:
(a) NPL 9510 for the root chord;
(b) NPL de ARC CP 1372 for the tip chord.

The geometric features of the horizontal stabilizer are shown in Table 2. The incidence angle was increased linearly from the stabilizer root to the stabilizer tip.

Table 2. Geometric features for the horizontal stabilizer.

C_r	5.82 m	α_r	-2.23 º	S	60.28 m^2
C_t	1.67 m	α_t	0 º	AR	5.95
Λ	35.16 º	ϕ	7.26 º	λ	0.28

The vertical stabilizer has the symmetric airfoil shown in Figure 9.

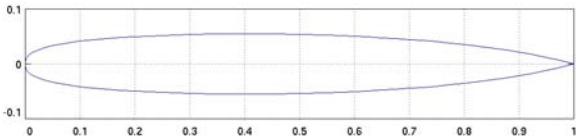

Figure 9. Symmetric supercritical airfoil NACA/LANGLEY N0011SC.

The geometric features for the vertical stabilizer are shown in Table 3.

Table 3. Geometric features for the vertical stabilizer.

C_r	8.42 m	C_t	2.44 m	λ	0.2897
Λ	42.8º	S	46.58 m^2	b	8.8 m

2.1. GEOMETRY OF THE ADAPTED WINGLETS

The winglets to be adapted in the wing tips of the aircraft are shown in Figure 10.

Figure 10. Winglets: (a) vortex diffuser; (b) tip fence.

The symmetric supercritical airfoil shown in Figure 9 is used in winglets tips. The geometric features of the winglets are shown in Table 4 respectively.

Table 4. Geometric features for winglets: (a) vortex diffuser; (b) tip fence.

Winglet	
C_r	2.15 m
C_t	0.88 m
Λ	56.32º
β	33.04º
S	2.8 m^2
λ	0.4074
b	2.12 m

(a)

Upper winglet		Lower winglet	
C_r	1.19 m	C_r	1.19 m
C_t	0.29 m	C_t	0.29 m
Λ	64.34 º	Λ	57.89 º
β	9.13 º	β	23.52 º
S	0.64 m^2	S	0.43 m^2
λ	0.25	λ	0.25
b	0.86 m	b	0.61 m

(b)

2.2. FLIGHT CONDITIONS

The flight conditions were taken for a typical cruise flight. These conditions are shown in the Table 5.

Table 5. Flight conditions and air properties.

V_o	236.38 m/s	μ	1.43 x 10^{-5} kg/ms
H	10.66 km (35,000 ft)	T	218.92 K
M	0.8	p	0.23 atm (23.3 kPa)
ρ	0.38 kg/m^3	a	296.9 m/s

The density presented in Table 5 is the nominal density in the far field. The density in the present analysis was modeled using the ideal gas equation of state. The modeling of the density using this equation of state has a good accuracy since the air atmospheric pressure used in the analysis is lower that the air critical pressure (p_c=3770 kPa) and the static temperature (temperature of the fluid under analysis) is higher than the air critical temperature (T_c=133 K).

2.3. ENGINE FEATURES

The engine velocities were calculated applying the momentum and continuity equations to the engine under analysis. Using a typical cruise thrust of 54.4 kN and a by-pass ratio of 5.31, the values listed in Table 6 were obtained.

Table 6. Engine features.

Core Flow	Static pressure	-0.05868 Pa
	Static temperature	504.82 K
	Velocity	480.5 m/s
	Density	0.1242 kg/m^3
	Flow area	0.49 m^2
By-pass flow	Static pressure	-0.03528 Pa
	Static temperature	214.1 K
	Velocity	367.3 m/s
	Density	0.3314 kg/m^3
	Flow area	1.282 m^2

3. NUMERICAL MODELING

The present analysis was performed using a commercial computer code. As the flow in the main wing is turbulent (the Reynolds number is 10^7), a turbulent model had to be used. Two-equation turbulence models offer a good compromise between numerical effort and computational accuracy. The k-ε turbulence model, with transport equations for turbulent kinetic energy, k and its dissipation rate, ε, was most widely used in the past. In order to improve the prediction of flow separation on smooth walls the Wilcox k-ω model was developed. This model solves two transport equations, one for the turbulent kinetic energy, k, and one for the turbulent frequency, ω. The advantage of the k-ω model is a new near-wall treatment which allows a smooth shift from a low-Reynolds number form to a wall function formulation. The main problem with the Wilcox model is its strong sensitivity to free stream conditions. In order to combine the advantages of the k-ω model near the surface and the k-ε model in the outer region, the BSL (baseline) model was developed. However the BSL model still fails to properly predict the onset and amount of flow separation from smooth surfaces. The main reason is that both models do not account for the transport of the turbulent shear stress. This results in an over-prediction of the eddy-viscosity. The proper transport behavior can be obtained by limiting to the formulation of the eddy-viscosity. This was done using the k-ω based SST (Shear Stress Transport) model. This model was used for all numerical calculations presented in this paper.

The governing equations to be solved were the continuity equation, the three momentum equations (in *x*, *y*, *z*), and the energy equation (including the viscous dissipation term for high velocities). These equations were solved in steady state for a compressible flow (the density is function of the pressure and the temperature), therefore, the equations were written in their conservative form.

Due to the complexity of modeling a compressible flow, the analyses for all numerical calculations were divided into two parts. The first part was in steady state and incompressible flow. The second part used the result of the incompressible flow as an initial guess value to reach convergence in the compressible flow. The convergence criteria was prescribed to $1x10^{-5}$.

Due to the symmetry of the aircraft the computational domain was reduced by one half. The grid was totally structured in the entire domain and it consisted of about 2 million elements. The grid of some parts of the aircraft is shown in Figure 11. The computational domain is a box with a length of 225 m, a thickness of 87 m and a height of 111 m. Figure 12 shows the computational domain of analysis.

(a)

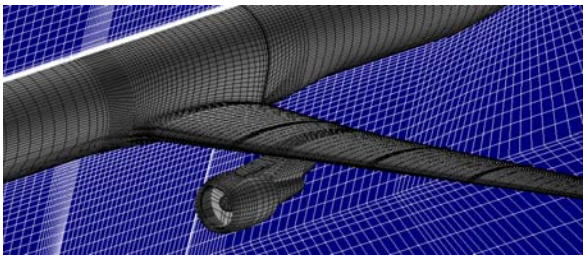

(b)

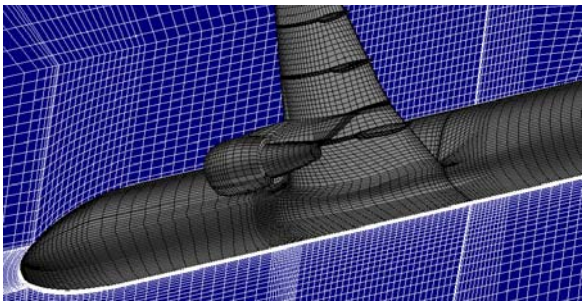

(c)

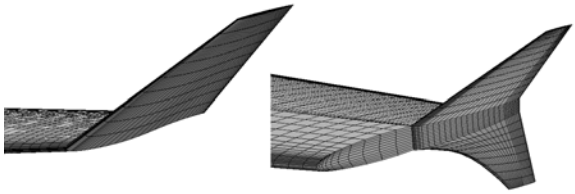

Figure 11. Grid of the aircraft: (a) upper wing view; (b) lower wing view; (c) vortex diffuser winglet (left), tip fence winglet (right).

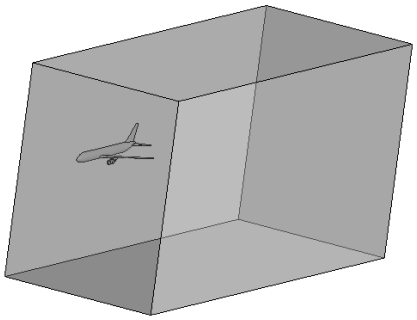

Figure 12. Computational domain.

At the inlet the flow direction were prescribed. The inlet velocity boundary was prescribed as 236.38 m/s (subsonic flow) with a static temperature of 218.92 K. The other boundary of the domain, the outlet boundary condition, was defined with a value of 0 Pa as an average static pressure (subsonic flow). The walls of the domain were prescribed as walls with free slip. The surfaces of the aircraft (with the exception of the inlet and outlet surfaces of fluid from the engine) were prescribed as adiabatic walls with no slip. The fan surface from the engine (inlet fluid to the engine) was prescribed as an outlet boundary condition to the domain, with a value of 0 Pa for the average static pressure. The by-pass and core surfaces of the engine (outlet flows from the engine) were prescribed as inlet velocity boundaries conditions for the computational domain. The inlet velocity boundary in the by-pass was prescribed as 367.3 m/s with a static temperature of 214.1 K (supersonic flow with a static pressure of -0.03528 Pa). The inlet velocity boundary in the core was prescribed as 480.5 m/s with a static temperature of 504.82 K (supersonic flow with a static pressure of -0.05868 Pa).

Three numerical cases were analyzed. The first one is for the B767, with a 1.7 million elements grid. The second one is for the B767 VDW, with a grid of 2 million elements, and the last one is for the B767 TFW, with a grid of 2 million elements. To determine the influence of the grid on the results a test case was performed. The starting grid consists of 3 million elements; the final grid consists of 2 million elements. The result for the wing lift force varies only 2.4%. It can be concluded that the grid of 2 million elements is accurate enough.

4. RESULTS

Figure 13 shows the static pressure and the streamlines from the wing and from the engine for the B767. The streamlines were plotted with the magnitude of velocity. The legend of the static pressure of the aircraft (Pa) is shown in Figure 14.

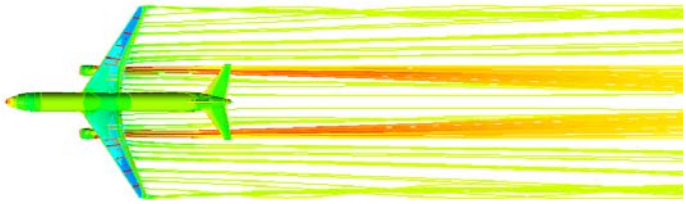

Figure 13. Wing and engine streamlines from the B767. The legend of the streamlines (m/s) is shown in Figure 15.

These streamlines show two different behaviors. The streamlines from the wing (location fuselage-engine) tend to surround the wake that was left by the fuselage. It means that the streamlines attempt to unite downstream. The rest of the streamlines from the wing (from engine-wing tip) have a direction towards the wing tip, and this behavior is greater near the wing tip.

Figure 14 a) shows that the streamlines passing through the zones of low pressure of the wing upper surface, have a direction towards the wing root. Afterwards when the flow passes through the zone of relative high pressure (due to the separation of the boundary layer on the wing upper surface near the trailing edge), it changes suddenly its direction, now towards the wing tip. Figure 14 b) shows that due to the zones of high pressure from the wing lower surface in the trailing edge, the streamlines have a direction towards the wing tip. Therefore the streamlines that left the wingspan (location engine-wing tip) have an overall direction towards the wing tip. On the other hand, Figure 15 b) shows that the flow that passes by the wing tip, tends to flow to the upper surface due to the zones of lower pressures, changing suddenly its direction. The direction of this flow over the upper surface is now towards the wing root. Hence, the rolling up of the flow is started in the wing tip when the flow coming from the wing tip (with direction towards the wing root) bonds with the flow coming from the wingspan (with direction towards wing tip). Figure 14 shows that the rolling up occurs in the wing tip. Finally, Figure 15 a) shows the two huge vortices emerging from each wing tip.

Figures 15, 17 and 18 shows the aircraft plotted with static pressure and the streamlines plotted with the magnitude of velocity. The legend of the static pressure of the aircraft (Pa) is shown in Figure 14.

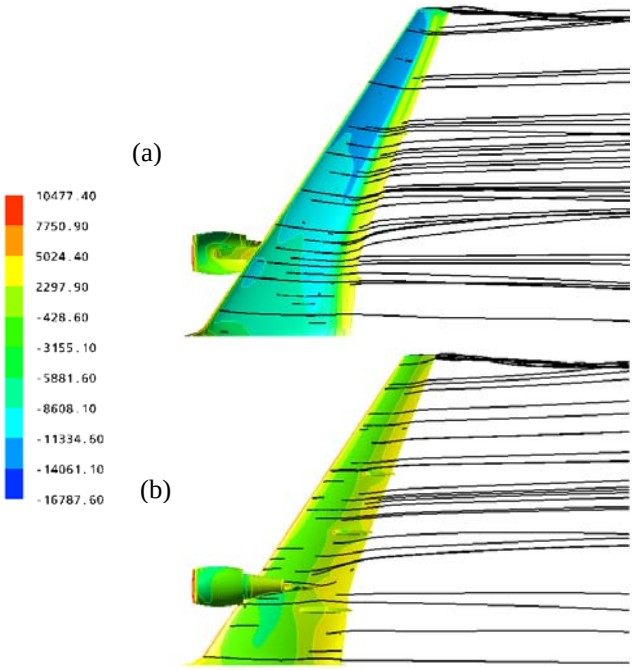

Figure 14. Static pressure from wing of B767 (Pa) and streamlines from the wing: (a) upper view; (b) lower view.

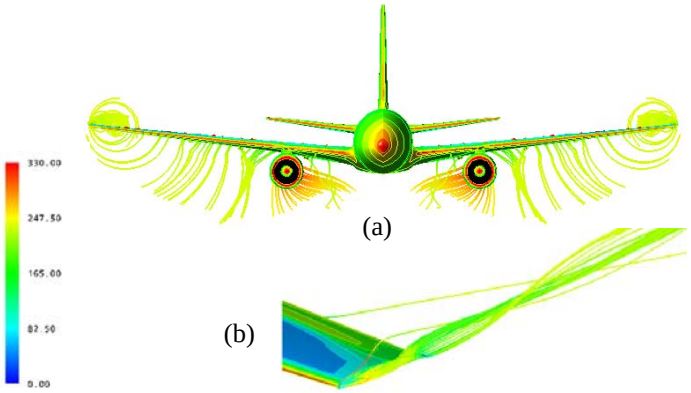

Figure 15. Wing tip vortices from B767 (m/s). (a) front view; (b) wing tip view.

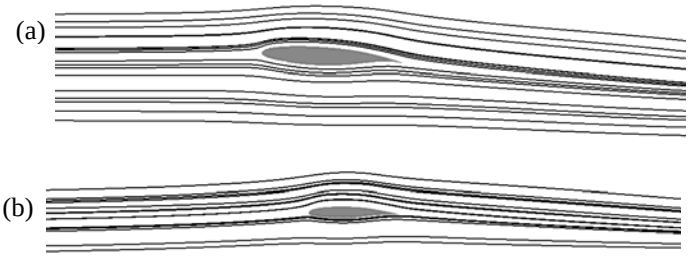

Figure 16. Streamlines of the wing for a location: (a) in the root chord; (b) in the tip chord.

Figure 16 a) shows that the flow upstream of the leading edge from the wing root airfoil has a horizontal direction. Figure 16 b) shows that the flow upstream of the leading edge from the wing tip airfoil has an upwash. Afterwards, in the trailing edge of the wing tip airfoil, a downwash flow is observed. This tendency to have an upwash flow upstream and a downwash flow in the trailing edge has the effect of tilting the free-stream direction. The downwash flow generates an induced velocity in the trailing edge along the span. This induced velocity is a component of the vortex generated in the wing tip, therefore the induced velocity is greater near the wing tip. Figures 17 and 18 show the streamlines for the B767 VDW and for the B767 TFW respectively.

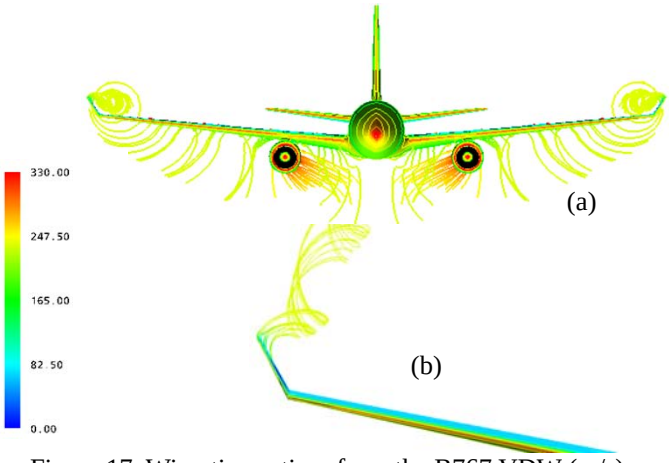

Figure 17. Wing tip vortices from the B767 VDW (m/s); (a) front view; (b) wing tip view.

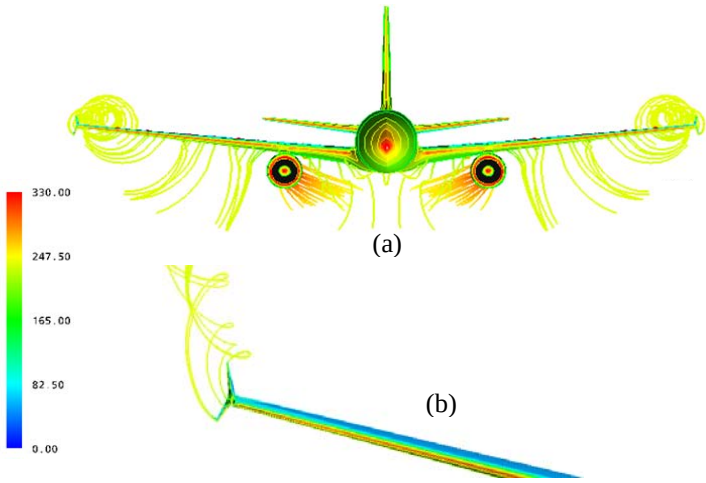

Figure 18. Wing tip vortexes from the B767 TFW (m/s); (a) front view; (b) wing tip view.

Figure 17 shows that the vortices are generated in the winglet tip. Due to the winglet span, the sweep angle and the angle that the winglet forms with the wing tip, the rolling up of the flow occurs in a zone of relatively higher pressure compared with the zone of lower pressure over the wing tip. In other words, the rolling up of the streamlines occurs now in a zone of less difference of pressures (negatives and positives) between the lower and upper surfaces. The same behavior is shown in Figure 18. The rolling up occurs in the upper winglet. The flow that emerges from the lower winglet tends to follow the rolling

up flow from the upper winglet. Figures 19, 20 and 21 show the v velocity component of the rolling up of the flow from the wing tip towards the downstream.

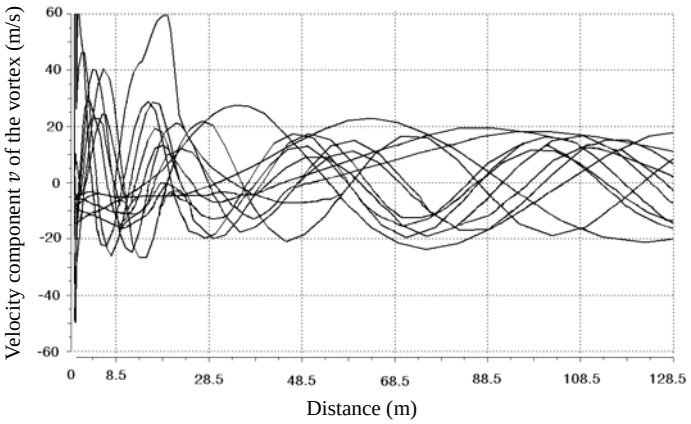

Figure 19. Vortex v velocity component of the wing tip vortex for the B767.

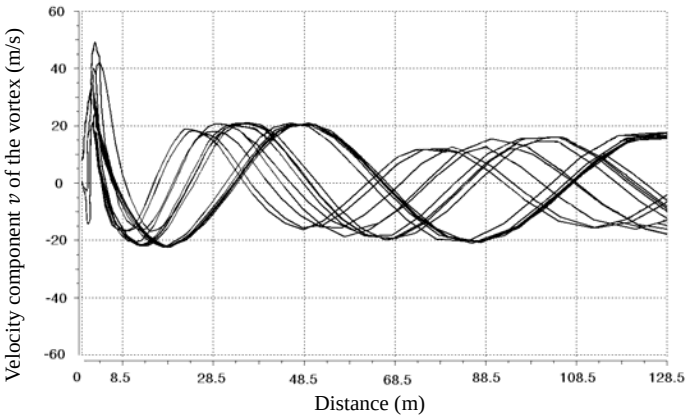

Figure 20. Vortex v velocity component of the wing tip vortex for the B767 VDW.

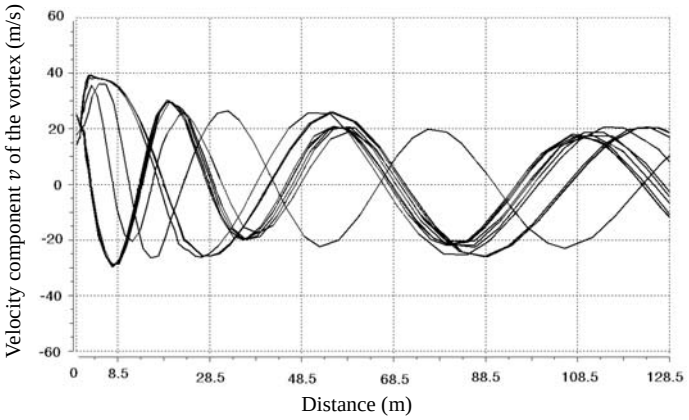

Figure 21. Vortex v velocity component of the wing tip vortex for the B767 TFW.

Figure 19 shows a rolling up with an almost sinusoidal behavior. It reaches maximum values up to 60 m/s. As this figure shows, each cycle is repeated at around 10 m downstream direction from the wing tip. Figure 20 shows a rolling up of the flow somehow more orderly. It reaches maximum values up to 45 m/s. As this figure shows, each cycle is repeated at around 30 m downstream direction from the wing tip. Figure 21 shows also a rolling up of the flow somehow more orderly compared with the rolling up of Figure 19. It reaches maximum values up to 40 m/s. As this figure shows, each cycle is repeated at around 20 m downstream direction from the wing tip

Figure 22 shows the average vortex core velocity for a distance starting in the wing tip to a distance downstream. It is shown that the vortex core velocity for the B767 started with a velocity of 58 m/s. Adib [1] mentions that the vortex core velocity of an Airbus A340 is near 60 m/s, validating the present results. The highest reduction in the vortex core velocity is for the B767 VDW. The B767 TFW has intermediate reduction in the vortex core velocity between the B767 and the B767 VDW.

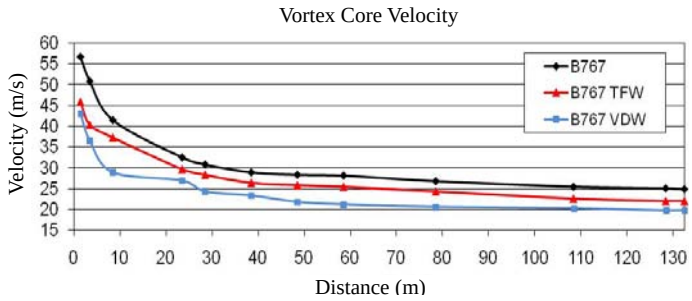

Figure 22. Magnitude and decay of the core wing tip vortex.

Table 7 shows the lift and drag forces and the overall ∈ for each wing of the aircrafts under analysis. The overall angle ∈ was calculated according to the forces components shown in Figure 3. Table 8 shows the total drag for each aircraft analyzed.

Table 7. Drag and lift force from the wing.

Wing	Drag force (kN)	Lift force (kN)	Overall ϵ
B767	100.7	1651.9	3.48º
B767 VDW	87.8	1691.5	2.97 º
B767 TFW	90.8	1677.6	3.10 º

Table 8. Total drag force from the aircraft.

Aircraft	Drag force (kN)
B767	190.0
B767 VDW	183.4
B767 TFW	185.2

According to the results shown in Tables 7 and 8, it is noted that the lowest aircraft and wing drag forces is for the B767 VDW, as well as the smallest angle ∈. Hence the lift should be the largest. Table 7 shows that the lift of the B767 VDW had the highest lift for all the cases. The B767 TFW had

intermediated values in drag reduction and lift increase compared to the B767 and the B767 VDW.

5. CONCLUSIONS

The rolling up of the flow in the wing tip started when the flow that left the wingspan with a direction towards the wing tip mixes with the flow that emerges in the wing tip to the upper surface with a direction towards the wing root. These differences in directions provoke that the flow rolls up in the wing tip. This produces an induced velocity in the trailing edge of the wing. As this induced velocity is a component of the vortex generated in the wing tip, the induced velocity is greater near the wing tip. The induced velocity causes the tilting of the resultant velocity along the wing airfoils with an angle $\in$. When winglets are used in the wing tips, the rolling up occurs in a zone of less difference of pressures between the lower and the upper surface. The reduction in the pressures differences causes a weaker strength in the generated vortex and therefore a decrease in the induced velocity in the trailing edge. As a consequence, the angle $\in$ is also reduced, decreasing the induced drag and increasing the lift. The best results were obtained for the B767 VDW, where there was a reduction in the total drag of the aircraft up to 3.6%, an increase in lift up to 2.4% and a reduction in the vortex core velocity up to 19%. The B767 TFW presented intermediated values between the B767 and the B767 VDW. The B767 TFW had a reduction in the total drag of the aircraft up to 1.6%, an increase in lift up to 1.9% and a reduction in the vortex core velocity up to 9%. Poisson-Quinton [9] mention that the tip fence winglet can reduce the drag of an aircraft up to 1.5% in cruise conditions. The vortex diffuser winglet presented best aerodynamics performance due to its higher winglet span. As a consequence the rolling up of the flow occurs in a zone far away from the wing tip, reducing the differences in pressures in the winglet tip. A higher winglet span presents best aerodynamic performance, but it also produces higher bending moments in the wing root, increasing the structural weight. The problem of induced drag reduction is clearly not an aerodynamic problem, it is a multidisciplinary design problem [10].

6. NOMENCLATURE

AR	Aspect ratio
a	Speed of sound (m/s)
b	Span (m)
B767	Boeing 767-300/ER
B767 VDW	Boeing 767-300/ER with adaptation of the vortex diffuser winglet
B767 TFW	Boeing 767-300/ER with adaptation of the tip fence winglet
C_r	Airfoil root chord (m)
C_t	Airfoil tip chord (m)
D	Drag force (N)
D_i	Lift-induced drag (N)
h	Height (m)
H	Altitude (km)
L	Lift force (N)
M	Mach number
p	Static air pressure (N/m^2)
q	Dynamic pressure (N/m^2)
S	Aerodynamic surface area (m^2)
T	Static air temperature (K)
U_∞	Free-stream direction (m/s)
v	Velocity component in *y* direction (m/s)
V_o	Aircraft velocity (m/s)
W	Induced velocity (m/s)
α	Angle of attack (degrees)
α_e	Effective angle of attack (degrees)
α_r	Root incidence angle (degrees)
α_t	Tip incidence angle(degrees)
β	Angle with the vertical (degrees)
Λ	Sweep angle (degrees)
ϵ	Downwash angle (degrees)
λ	Taper ratio
ϕ	Dihedral angle (degrees)
ρ	Air density (kg/m^3)
μ	Air dynamic viscosity (kg/ms)
Γ	Circulation (m^2/s)

7. REFERENCES

[1] J. Adib, Interaction between the Wing Trailing Vortex and the Engine Plume, Cranfield University, MSc Thesis, Cranfield University, 2006.

[2] J. Boehrer, CFD Study of Wing Tip Vortex Generation, MSc Thesis, Cranfield University, 2005.

[3] Hoeijmakers, H.W.M., Vortex Wakes in Aerodynamics, In the Characterization and Modification of Wakes from Lifting Vehicles in Fluid, AGARD CP 584, 1996.

[4] John J. Bertin, Michael L. Smith, Aerodynamics for Engineers, Second Edition, Prentice Hall, 1989.

[5] Ilan Kroo, Drag Due to Lift: Concepts for Prediction and Reduction, Journal of Fluid Mechanics, Vol. 33, pp. 587-617, 2001.

[6] Heyson HH, Roebe GD, Fulton CL., Theoretical Parametric Study of the Relative Advantages of Winglets and Wing-tip Extensions, NASA TP 1020, Natl. Advis. Comm. Aeronaut., Hampton, VA, 1977.

[7] Lowson MV., Minimum Induced Drag for Wings with Spanwise Camber, AIAA J. Aircr., 27:627–31, 1990.

[8] Von Karman T, Burgers JM., General Aerodynamic Theory Perfect Fluids, Airfoils and Airfoil Systems of Finite Span, In Aerodynamic Theory, ed. WF Durand, Vol. 2, Div. E. Berlin: Julius Springer, pp. 367, 1935.

[9] Poisson-Quinton P., Parasitic and Interference Drag Prediction and Reduction, In Aircraft Drag Prediction and Reduction, AGARD rep. 723, Rhode-St-Genese, Belg., pp. 6-1-6-27. Neuilly-sur- Seine, France: AGARD, 1985.

[10] Jones RT., Improving the Efficiency of Smaller Transport Aircraft, NASA TM 85992, Natl. Aeronaut. Space Admin. Ames Res. Cent., Moffett Field, Calif., 1984.